NANO LETTERS
Letter
Cite This: Nano Lett. 2018, 18, 7469−7477
pubs.acs.org/NanoLett

Thermal Boundary Conductance Across Heteroepitaxial ZnO/GaN Interfaces: Assessment of the Phonon Gas Model

John T. Gaskins,[†] George Kotsonis,[‡] Ashutosh Giri,[§] Shenghong Ju,[∥,⊥] Andrew Rohskopf,[#] Yekan Wang,[▽] Tingyu Bai,[▽] Edward Sachet,[‡] Christopher T. Shelton,[‡] Zeyu Liu,[○] Zhe Cheng,[#] Brian M. Foley,[#] Samuel Graham,[#,◆] Tengfei Luo,[○,¶] Asegun Henry,[#,◆,■] Mark S. Goorsky,[▽] Junichiro Shiomi,[∥,⊥] Jon-Paul Maria,[‡] and Patrick E. Hopkins*[,§,▲,▼]

[†]Department of Mechanical and Aerospace Engineering, University of Virginia, Charlottesville, Virginia 22904, United States
[‡]Department of Materials Science and Engineering, North Carolina State University, Raleigh, North Carolina 27695, United States
[§]Department of Mechanical and Aerospace Engineering, University of Virginia, Charlottesville, Virginia 22904, United States
[∥]Department of Mechanical Engineering, The University of Tokyo, Bunkyo, Tokyo 113-8656, Japan
[⊥]Center for Materials research by Information Integration (CMI2), Research and Services Division of Materials Data and Integrated System (MaDIS), National Institute for Materials Science (NIMS), 1-2-1 Sengen, Tsukuba, Ibaraki 305-0047, Japan
[#]George W. Woodruff School of Mechanical Engineering, Georgia Institute of Technology, Atlanta, Georgia 30332, United States
[▽]Department of Materials Science and Engineering, University of California, Los Angeles, California 90095, United States
[○]Department of Aerospace and Mechanical Engineering, University of Notre Dame, Notre Dame, Indiana 46556, United States
[◆]School of Materials Science and Engineering, Georgia Institute of Technology, Atlanta, Georgia 30332, United States
[¶]Center for Sustainable Energy of Notre Dame (ND Energy), University of Notre Dame, Notre Dame, Indiana 46556, United States
[■]Heat Lab, Georgia Institute of Technology, Atlanta, Georgia 30332, United States
[▲]Department of Materials Science and Engineering, University of Virginia, Charlottesville, Virginia 22904, United States
[▼]Department of Physics, University of Virginia, Charlottesville, Virginia 22904, United States

Supporting Information

ABSTRACT: We present experimental measurements of the thermal boundary conductance (TBC) from 78−500 K across isolated heteroepitaxially grown ZnO films on GaN substrates. This data provides an assessment of the underlying assumptions driving phonon gas-based models, such as the diffuse mismatch model (DMM), and atomistic Green's function (AGF) formalisms used to predict TBC. Our measurements, when compared to previous experimental data, suggest that TBC can be influenced by long wavelength, zone center modes in a material on one side of the interface as opposed to the "'vibrational mismatch"' concept assumed in the DMM; this disagreement is pronounced at high temperatures. At room temperature, we measure the ZnO/GaN TBC as 490[+150,−110] MW m^{-2} K^{-1}. The disagreement among the DMM and AGF, and the experimental data at elevated temperatures, suggests a non-negligible contribution from other types of modes that are not accounted for in the fundamental assumptions of these harmonic based formalisms, which may rely on anharmonicity. Given the high quality of these ZnO/GaN interfaces, these results provide an invaluable, critical, and quantitative assessment of the accuracy of assumptions in the current state of the art computational approaches used to predict phonon TBC across interfaces.

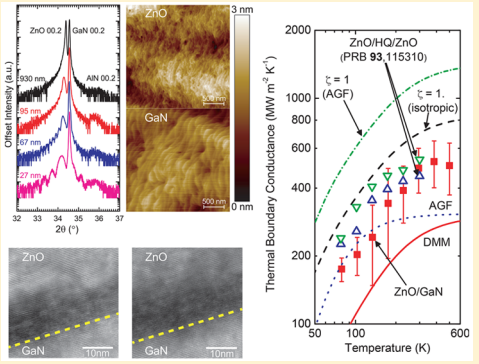

KEYWORDS: *Thermal boundary conductance, DMM, AGF, gallium nitride, zinc oxide,, phonon gas model, interfacial thermal transport*

The thermophysical property defining thermal transport across an interface between two materials is often termed the thermal boundary conductance (TBC), frequently approximated through phonon gas theory as[1]

$$h_K = \frac{1}{4}\sum_j \int_{\mathbf{k}} C_j(\mathbf{k}) v_{g,j}(\mathbf{k}) \zeta(\mathbf{k}) d\mathbf{k} \quad (1)$$

where j is the phonon polarization index, $\mathbf{k}$ is the wave-vector, v_g is the group velocity, and ζ is the phonon transmission coefficient. According to eq 1, the maximum TBC across an

Received: July 11, 2018
Revised: September 30, 2018
Published: November 9, 2018

DOI: 10.1021/acs.nanolett.8b02837
Nano Lett. 2018, 18, 7469−7477

interface can be achieved by engineering ζ to approach unity. However, TBC is often assumed to decrease as the ratio of Debye temperatures of the materials comprising the interface decreases; in this case, the materials become more "vibrationally mismatched" and thus the transmission coefficient reduces.[2−8] This vibrational matching concept was inferred from the well understood and proven behaviors that occur in the elastic limit, where one can analyze long wavelengths. In this elastic/harmonic limit, only vibrations that are closely matched in frequency are able to transmit their energy across an interface. This basic concept that only modes that are frequency matched can transmit energy has formed the backbone of what is presumed to be known about TBC. Although this result is only rigorously true in the elastic limit, it is often extrapolated to be true for all phonons and temperatures and forms the basis of the diffuse mismatch model (DMM),[8] which, as with eq 1, is also rooted in the assumptions of the "phonon gas model" (PGM). Under this formalism, at a heterogeneous interface ζ can never approach unity due to the differing vibrational densities of states. However, recent work has demonstrated that at epitaxial or well-bonded interfaces TBC can approach this maximal limit.[2,5,9] These experimental works draw into question the validity of the DMM and other PGM-based approaches in predicting the TBC across material interfaces. Similarly, these questions have recently been raised in computational studies.[10,11]

In principle, a direct comparison of these models to experimental data should provide a check of the ability of these theoretical approaches to correctly predict the phonon driven TBC. Indeed, several groups have recently provided this comparison to assess the validity of computational approaches based on the DMM or Atomic Green's Function (AGF) formalisms.[12−14] However, these works along with the overwhelming majority of measurements of TBC across interfaces have focused on metal/nonmetal interfaces.[4,13,15−17] Arguments rooted in the assumption that electron−phonon scattering at metal/nonmetal interfaces contributes to TBC have often been made to explain models and data for metal/nonmetal interfaces.[18−27] While the validity of these electron−phonon assumptions have been challenged via selected experiments,[3,28−30] the presence of this unverified interfacial heat transfer mechanism certainly calls into question direct comparisons of metal/nonmetal TBC to the PGM or AGF models, effectively leaving these phonon TBC models unvetted.

The assessment offered in this work is important as it examines an import basis of the PGM, namely that PGMs are rooted in the concept of phonon transmissivity across an interface. Both DMM and AGF are rooted in a Landauer formalism and treat the TBC as a transmission of phonons. In the two extremes of computational rigor presented in this work, the DMM representing low-level and AGF high, the DMM treats phonons as particles whereas the AGF accounts for the wave nature of phonons. It is important to note that in both models, the TBC is treated as a transmission with only elastic interactions. The results in our present work demonstrate that the elastic phonon transmission approach to model the TBC will not capture experimental data regardless of the rigor of the model calculations.

Knowing this, a measurement of TBC across an interface of adjacent crystalline nonmetals would enable an assessment of the ability of DMM and AGF models to predict phonon transport across interfaces. However, previous works reporting measurements of nonmetal/nonmetal TBC across single interfaces (i.e., not interpreted from superlattice measurements or across transition layer interfaces) are lacking and limited to highly disordered or amorphous interfaces.[31−34] It is well-known that pronounced interfacial disorder can lead to changes in TBC[15], and as a result the aforementioned nonmetal/nonmetal interface studies are not ideal to validate phonon computational formalisms, which can not take into account nonidealities at the interface.

In this work, we overcome this void in the literature by studying the TBC across ZnO/GaN interfaces. We experimentally measure the TBC across isolated heteroepitaxially grown ZnO films on GaN substrates from 78−500 K. We make note that the term isolated interface is meant to specify that we can directly measure the TBC of the ZnO/GaN interface as opposed to deriving the TBC from the thermal conductivity of samples with a high density of internal interfaces, such as superlattices. High lattice matching and subsequent heteroepitaxial growth ensure high crystalline quality of the ZnO films. Experimentally measured TBCs are directly compared to the DMM using first-principles derived phonon dispersions and AGF calculations based on first-principles force constants. Our measurements show high values for ZnO/GaN TBCs that exceed the values predicted by AGF and DMM calculations by nearly a factor of 2 at elevated temperatures. This difference between experiment and computation suggests the basic assumptions governing these formalisms are not suitable to predict the phonon TBC; this points to the potential existence of anharmonic phonon interactions enhancing the TBC at this ZnO/GaN interface, a process that is not rigorously accounted for in DMM or AGF simulations. We compare our measured ZnO/GaN TBC to calculations of the theoretical maximum predicted under various assumptions, along with previously derived TBCs from measurements of ZnO/hydroquinone (HQ) superlattices.[9] In comparison to various models and previous data, our results suggest TBC may be intrinsic to the phonon modes in the ZnO and not necessarily related to a "transmission" of modes restricted by the vibrational states on the other side of the interface. This mechanism of TBC being inherent to phonon modes in the ZnO can not be predicted by PGM-based formalisms. It is important to note that these results may also be explained by the presence of anharmonic interactions at the interface but that we can not yet separate which mechanism or combination of mechanisms are responsible for the differences between experiment and computation.

ZnO thin films of thickness between 5−930 nm were grown heteroepitaxially on a Ga-polar GaN wafer by pulsed-laser deposition. The GaN wafer was prepared on a [0001]-sapphire wafer by metal−organic chemical vapor deposition employing an AlN buffer layer.[35,36] Film structure, roughness, and thickness were characterized by X-ray diffraction (XRD) including reciprocal space maps, atomic force microscopy (AFM), and X-ray reflectivity (XRR). Figure 1a shows offset $2\theta-\omega$ XRD scans of the ZnO and GaN [002] reflections for a representative subset of the films. A strong ZnO [002] reflection can be seen beside the GaN [002] peak, indicating the films adopt the [001] orientation of the GaN. Pendellosung fringing can be seen in some of the XRD patterns, a result of X-ray interference from the ZnO thickness, typically indicative of high crystal quality and smooth interfaces.[37] A 2θ-peak shift to lower angles (larger interplanar

DOI: 10.1021/acs.nanolett.8b02837
Nano Lett. 2018, 18, 7469−7477

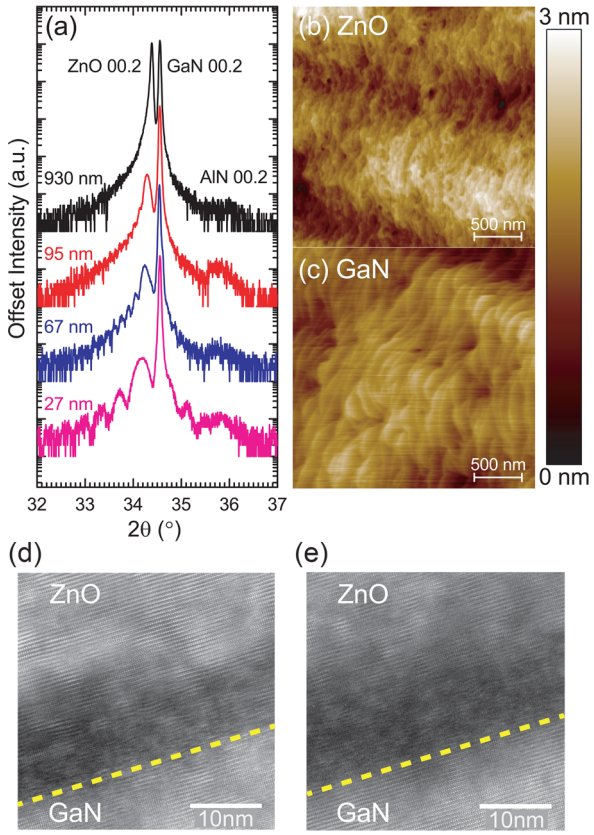

Figure 1. (a) XRD patterns for ZnO grown on GaN with various thicknesses, (b) AFM data for 95 nm of ZnO, (c) AFM data for the bare GaN wafer, and HRTEM images at the ZnO/GaN interface for the 180 nm (d) and 95 nm (e) ZnO samples where the dotted yellow line in both (d,e) denotes the ZnO/GaN interface.

spacing at lower thickness) can also be seen in Figure 1a. This shift indicates that thin ZnO films experience in-plane compressive epitaxial strain, while thicker ZnO films tend to relax toward their bulk lattice parameter, as confirmed with reciprocal space maps (see Supporting Information). Long range 2θ–ω scans (see Supporting Information) indicate a small amount of [110]-oriented ZnO grains at thicknesses above 100 nm, but thinner films exhibit a pure [001] orientation, implying that the [110] ZnO nuclei precipitate away from the ZnO/GaN interface.

Representative AFM data for the 95 nm thick ZnO film and the GaN wafer are shown in Figure 1b,c, respectively. The GaN surface exhibits a step-terrace morphology and the ZnO films adopt a comparable morphology with less distinct but still observable step edges. The RMS surface roughness of all ZnO films was ∼1 nm or less and that of the GaN was <1 nm, determined by AFM image analysis. Together, the XRD and AFM data suggest heteroepitaxy and ZnO/GaN interfaces with low dislocation density. While our structural characterization indicates high crystalline quality of the ZnO, the small lattice mismatch necessitates at least some volume of defected region near the ZnO/GaN interface. In order to further investigate this interface, cross-sectional transmission electron microscopy (TEM) samples were prepared using the focused ion beam lift-out technique. The samples, including both ZnO and GaN layers as well as the interface between the two materials, were extracted from the bulk sample and thinned to less than 100 nm. The high-resolution TEM images of the ZnO/GaN interface show an approximately 10−12 nm defective region in the ZnO, shown in Figure 1d,e for the 95 and 180 nm samples, respectively. It should be noted that the presence of dislocations at an interface may influence the thermal boundary conductance. However, previous works have shown that the dislocation density at a ZnO/GaN interface with films grown under similar conditions was $2 \times 10^8/\mathrm{cm}^2$. Another prior work demonstrated that dislocation densities of this magnitude had little to no influence on the thermal boundary conductance between epitaxially grown GaSb and GaAs.[32] In this regard, we expect the presence of dislocations at the ZnO/GaN interface to have a minimal effect on the TBC. There is negligible interface mixing as determined via energy dispersive X-ray spectroscopy mapping and, thus we conclude that the ZnO/GaN interfaces are relatively chemically abrupt and no separate phases are formed near the interface. Additionally, $(1\bar{1}00)$ two beam images at the interface shows crystalline disorder from dislocations whereas the ZnO material above this interface layer, as well as the GaN layer below it, exhibit high crystalline quality. Regardless of this relatively dislocation-dense interfacial region, the ZnO and GaN are crystalline, including in regions near the interface. Further TEM images and details on analysis can be found in the Supporting Information. For ZnO films less than 100 nm thick, XRR was employed for thickness determination.[38] Fitting of the XRR data provided ZnO layer thickness and yielded surface roughness that agree with AFM data. For the 180 and 930 nm thick films, XRR was not able to resolve thickness oscillations and, as such, selective etching and AFM profilometry of a companion film, grown in the same growth as the thermally characterized films, were used to determine the thickness.

Our thermal measurements were carried out using time domain thermoreflectance (TDTR), a technique that is described in detail elsewhere.[31,39,40] We first measure a piece of the same GaN on sapphire wafer on which the ZnO films were grown in order to measure both the GaN/sapphire TBC as well as the thermal conductivity, κ, of the GaN. We measure $\kappa_{GaN} = 159 \pm 12$ W m^{-1} K^{-1}, in line with previous measurements of high quality GaN with thickness of ∼1 μm.[41] These values are used in all subsequent analyses discussed below and has the effect of reducing the number of unknowns in our analysis to three: $h_{K,Al/ZnO}$, κ_{ZnO}, and $h_{K,ZnO/GaN}$. In order to determine the thermal conductivity of our ZnO, we measure a 930 nm thick film. This thickness ensures we are only sensitive to the thermal conductivity of the ZnO and $h_{K,Al/ZnO}$, and not to $h_{K,ZnO/GaN}$. The thick ZnO film yields a thermal conductivity of $\kappa_{ZnO} = 53.4 \pm 4$ W m^{-1} K^{-1}, similar to values found in literature for high quality ZnO (refs 42−44) and in line with recent computational work.[45] Both the GaN control and thick ZnO thermal conductivity were independently tested and verified via TDTR at the University of Virginia and Georgia Institute of Technology. It should be noted there are a host of lower literature values for thin film ZnO that are highly influenced by the microstructural features present in the films, namely the presence of grain boundaries, which may act as phonon scattering sites.[46,47]

In order to obtain $h_{K,ZnO/GaN}$, we test films with thickness of 180 and 95 nm. Taking κ_{ZnO} from the thick film leaves us with two unknown parameters in the thermal model, $h_{K,ZnO/GaN}$ and $h_{K,Al/ZnO}$, which we can determine by fitting $h_{K,Al/ZnO}$ with the in-phase signal, V_{in}, and $h_{K,ZnO/GaN}$ with the ratio of $-V_{in}/V_{out}$. We iterate these values into the opposing thermal models until

DOI: 10.1021/acs.nanolett.8b02837
Nano Lett. 2018, 18, 7469−7477

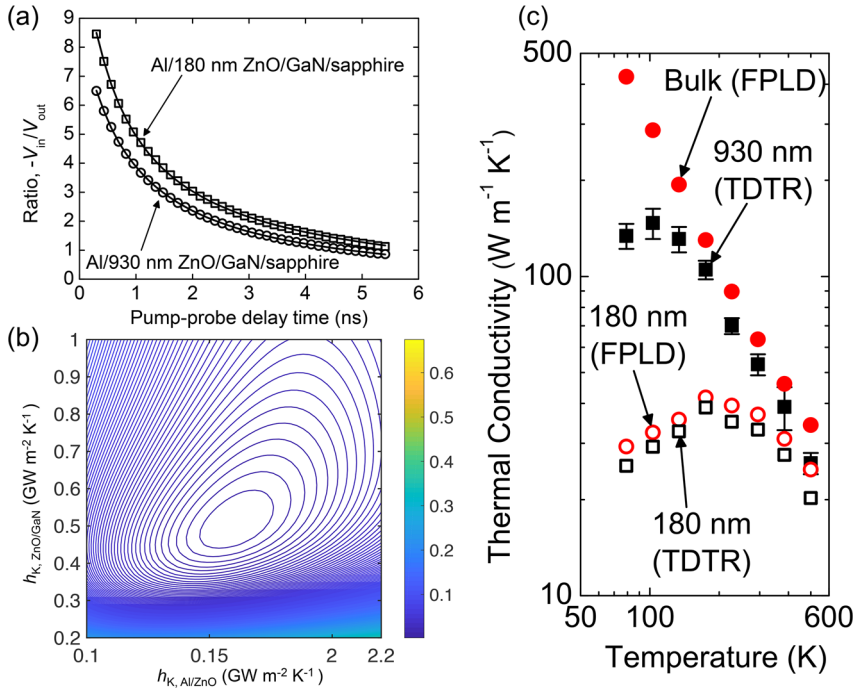

Figure 2. (a) Experimental data (open symbols) and the best fits to our thermal model (solid lines) for the 180 and 930 nm thick ZnO films. (b) Sensitivity contour plots for the 180 nm thick film for $h_{K,ZnO/GaN}$ as a function of $h_{K,Al/ZnO}$. The lowest value of the contour lines indicates the combinations of thermal parameters that lie within a 95% confidence interval. As is clear from the sensitivity contour plot, a relatively confined range of values for $h_{K,ZnO/GaN}$ and $h_{K,Al/ZnO}$ can produce best fits to the TDTR data, confirming our uncertainty bounds in our measurements of $h_{K,ZnO/GaN}$ in the 180 and 95 nm thick films. (c) Measured thermal conductivity of the 930 nm ZnO films (filled squares) compared to predictions of bulk ZnO thermal conductivity via first-principles lattice dynamics (FPLD, filled circles). Using a series resistance model that accounts for $h_{K,ZnO/GaN}$, we then compare the effective thermal conductivities of the measured 180 nm films (open squares) and that predicted from FPLD (open circles). The agreement supports our analysis procedure that assumes the thermal conductivity of the ZnO is reduced due to a TBC at the ZnO/GaN interface.[48]

the values converge, yielding an average for these films of moderate thickness of $h_{K,ZnO/GaN}$= 490[+150,−110] MW m^{-2} K^{-1}. This value is among the highest nonmetal/nonmetal room-temperature value reported in literature despite the aforementioned 10−12 nm defective region at the interface. Exemplary TDTR data and the model fits for the 930 and 180 nm films are shown in Figure 2a. Figure 2b shows the results from a contour plot analysis that demonstrates the mean square deviation of the thermal model to the TDTR data ($-V_{in}/V_{out}$) for various combinations of $h_{K,ZnO/GaN}$ and $h_{K,Al/ZnO}$ as input parameters in the model for the 180 nm film. The lowest value of the contour lines indicates the combinations of thermal parameters that lie within a 95% confidence interval. As is clear from the sensitivity contour plot, a relatively confined range of values for $h_{K,ZnO/GaN}$ and $h_{K,Al/ZnO}$ can produce best fits to the TDTR data, confirming our uncertainty bounds in our measurements of $h_{K,ZnO/GaN}$ in the 180 and 95 nm thick films. We further confirm these reported values for $h_{K,ZnO/GaN}$ through measurements on the thinner ZnO films with thicknesses of 5, 10, 19, 27, 42, and 66 nm, discussed in the Supporting Information.

In light of the measurements and the relevant mean free paths in ZnO, it is important to discuss the nature of the phonon population impinging on the ZnO/GaN interface. The mean free paths in ZnO, which can be found in the Supporting Information, can be larger than the thicknesses of our films. In this case, the TBC at the ZnO/GaN interface could be influenced by a portion of phonon frequencies in ZnO that are impinging on the interface after traversing through the ZnO ballistically. However, we assume that the ZnO phonons are thermalized at the Al/ZnO interface and as such the spectrum of phonons transferring heat across the ZnO impinging on the ZnO/GaN interface are most likely a thermalized distribution. Given this assumption, there are some portion of phonons traversing the ZnO ballistically and some portion traveling diffusively through the ZnO. That all samples regardless of thickness yield the same result, or same lower bound, within error suggests the TBC at the interface is not influenced by ballistic phonon transport in the ZnO.

To allow for further investigation of the transport properties at this well matched interface, we turn to temperature dependent measurements of $h_{K,ZnO/GaN}$. Relevant thermophysical properties for the temperature dependent measurements and analyses were taken from a combination of measurements on control samples, namely the thick GaN and ZnO samples, and a variety of existing literature.[42,49−54] As a validation of our analysis procedure, we compare the measured thermal conductivity of ZnO to those predicted via first-principles lattice dynamics (FPLD).[45] Figure 2c shows that the measured thermal conductivities of our thickest ZnO film (930 nm) agree well with the FPLD predictions at higher temperatures. At cryogenic temperatures, the deviation between the TDTR data and FPLD predictions is most likely due to size effects in the 930 nm film that are more pronounced at these lower temperatures. To test our assumptions regarding the role of size effects and our ability to extract the ZnO/GaN TBC in our TDTR analysis, we calculate κ_{ZnO} for the 180 nm thick film using FPLD with a boundary resistance in series, which we

DOI: 10.1021/acs.nanolett.8b02837
Nano Lett. 2018, 18, 7469−7477

take from our measured data, given by $\kappa_{effective} = (180 \times 10^{-9}$ m/$\kappa_{FPLD,bulk} + 1/h_{K,ZnO/GaN})^{-1}$. We compare these predictions to the measured effective thermal conductivities via TDTR. The agreement between these FPLD predictions and our measured data shown in Figure 2c give additional credence to our TDTR fitting procedure used to measure $h_{K,ZnO/GaN}$ over a range of temperatures; namely that the thermal conductivity of the ZnO thin films is reduced due to the finite TBC at the ZnO/GaN interface. Specifically, we analyze our data in the picture where the ZnO has an intrinsic thermal conductivity and any size effects that would commonly be reported for thin film ZnO are driven by the TBC at the ZnO/GaN interface.[48] The slight disagreement between the FPLD model and our TDTR data may be due to atomic defects in the ZnO, as the FPLD simulations are based on a perfect crystal. This is in line with the defective region we have shown at the ZnO/GaN interface, which may account for this difference between the model and measurements.

Figure 3 shows the results for $h_{K,ZnO/GaN}$ as a function of temperature. We also plot experimental data from our recent

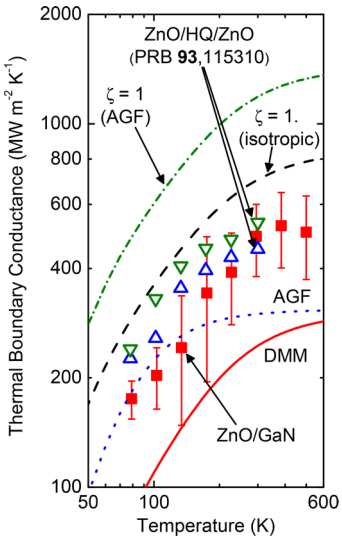

Figure 3. Measured ZnO/GaN TBC as a function of temperature (filled squares) compared to previous data measured across ZnO/HQ/ZnO interfaces (open triangles),[9] DMM and AGF predictions of the ZnO/GaN TBC (solid and dotted lines, respectively), and the maximum TBC predicted via eq 1 (assuming isotropy, dashed line) and this maximum TBC assuming a more precise shape to the Brillouin Zone (dot-dashed line).[45] At low temperatures, the agreement between the data and AGF and their disagreement with the DMM is ascribed to the failure of the DMM to account for the effective interfacial transport of long wavelength modes. The disagreement between the measured data and both the AGF and DMM (and the convergence of these models) suggest that inelastic scattering among different mode energies could be contributing to the ZnO/GaN TBC, a phenomenon that is not rigorously accounted for in our DMM and AGF formalisms assumed here.

work showing TBC across ZnO/HQ/ZnO interfaces extracted from thermal conductivity measurements of organic/inorganic multilayers grown via atomic/molecular layer deposition.[9] The similarities in TBCs, in both magnitude and temperature trends, suggest similar interfacial heat transport mechanisms driving the TBC. In the case of the ZnO/HQ/ZnO, the results suggested that the TBC was driven by the phonon flux in the ZnO. The similarity in our current values for this heterogeneous ZnO/GaN interface suggest the same: namely, the heat transport mechanisms driving the TBC across this ZnO/GaN epitaxial interface are intrinsic to the ZnO, an observation that is contradictory to the DMM and other PGM-based theories. Recent works[55,56] have suggested that the TBC across ideal interfaces can be driven by near perfect transmission of long wavelength, zone center phonons. It should be noted that recent works have shown that long-wavelength phonons at interfaces can in fact have a transmissivity close to unity.[56] This is in disagreement with theories rooted in the PGM, such as the DMM and other Landauer-based formalisms, that assume vibrational mismatch between two materials' densities of states can impact transmission of all phonon wavelengths and do not capture the wave-based nature of phonon transport.[57] Even so, AGF calculations take into account the wave nature of phonons and for long-wavelength phonons at perfect interfaces would naturally capture a higher transmissivity than is predicted via the DMM. This difference in how the DMM and AGF treat phonons explains the discrepancy between the DMM and AGF seen in Figure 3. Furthermore, our results support these aforementioned works[55,56] and suggest that at "perfect" interfaces the conductance can be intrinsic to one of the materials adjacent to the interface, in our case, ZnO.

We more quantitatively analyze our measured TBC data and assess the viability of AGF and PGM-based DMM assumptions by calculating the TBC via the DMM and AGF. We specifically target these two modeling formulations for a variety of reasons. The DMM is arguably the most widely used tool to calculate TBC at the interface between two materials, and offers a relatively simple assessment of TBC. Conversely, the AGF represents the other end of the extremes of computational rigor for modeling TBC as the AGF takes into account the atomic arrangement and interatomic potentials at and near the interface. It is important to note that, while the atomic nature of the interface is captured in AGF simulations, AGF still relies on the principle of phonon transmissivity. As such, both of these models, while vastly varying in rigor, rely on a phonon transmission concept and in the implementation of the models in this work cannot account for anharmonic interaction that may take place at the interface. First, we calculate the ZnO/GaN TBC with the DMM assuming an isotropic Brillouin Zone, an assumption that is arguably the most widely applied in DMM predictions.[1,5,8,58] The details of these calculations are further discussed in the Supporting Information but we note that we calculate the DMM via a polynomial fit to the phonon dispersion of ZnO and GaN in the $\Gamma \rightarrow M$ direction.[59,60] The DMM underpredicts the measured $h_{K,ZnO/GaN}$ by nearly a factor of 2 across the entire temperature range. It should be noted that our assumption of Brillouin Zone isotropy may certainly be playing a role in this disagreement as anisotropy in the crystal structure can affect TBC.[61−64] However, as previously discussed, our data also suggest that the fundamental assumptions driving the DMM can not capture the TBC at this heteroepitaxial ZnO/GaN interface, so this disagreement is not surprising.

We also calculate the ZnO/GaN TBC using AGF, as shown in Figure 3. Our AGF calculations include the exact atomic level detail of the interface, in comparison to the DMM which is limited in this atomic-level description. We note that direct comparisons between AGF calculations and an appropriately matched experimental measurement of an isolated nonmetal-nonmetal TBC are, to the best of our knowledge, nonexistent.

DOI: 10.1021/acs.nanolett.8b02837
Nano Lett. 2018, 18, 7469−7477

Thus, our results herein for an AGF prediction of the ZnO/GaN interface provide a critical comparison that has been absent in the literature and we believe this is the first true test of the underlying theory of the AGF method, via a direct comparison to experiments, whereby there is minimal discrepancy between the simulated and measured structures. It is important to note that, although we have identified a disordered region near the ZnO/GaN interface as previously discussed, our interfaces are still single crystalline, justifying this direct comparison with AGF. Our AGF calculations were performed ab initio using density function theory (DFT). The electronic structure calculations were performed using Quantum ESPRESSO.[65] The general details associated with the AGF implementation are well described elsewhere,[66−69] and our specific assumptions are outlined in the Supporting Information; the results of these calculations are shown in Figure 3. In general, the AGF calculations capture the low temperature values but underpredict the trends and values at high temperatures.

Unlike the DMM, the AGF formalism accounts for the wave-like nature of phonon transport and naturally captures phonon transport processes typically associated with traditionally assumed acoustic mismatch theories;[8,70,71] that is, AGF can account for the fact that long wavelength phonons can efficiently transfer energy across interfaces more so than short wavelength phonons,[72,73] a phenomena that has been theorized previously.[32,56,74,75] It is of note that the DMM does not account for this effect and assumes all phonons scatter diffusively at interfaces, thus underpredicting the contribution of long wavelength phonons to TBC. This has the potential to explain the disagreement between the AGF and DMM predictions at low temperatures and supports these aforementioned previous theories that long wavelength phonons can effectively transfer energy across heterogeneous interfaces,[32,56,74,75] and do not obey DMM-based constraints.

At higher temperatures the DMM and AGF calculations converge, while still underpredicting the experimental data by nearly a factor of 2. A potential source of this underpredicition has often been ascribed to inelastic scattering at the interface, where anharmonic interactions among multiple phonons can open up additional parallel pathways for increases to TBC.[3,55,76−80] Given that both our AGF and DMM calculations only assume harmonic interactions, this indeed could explain the discrepancy between the models and our measured data. More specifically, especially given the rigor of our AGF calculations and the applicability of its direct comparison to our experimental data, inelastic scattering processes are most likely contributing to the TBC at the ZnO/GaN interface at elevated temperatures.

Figure 3 also shows the calculations for the maximum possible TBC, calculated both via eq 1 with $\zeta = 1$, which assumes an isotropic Brillouin Zone in the $\Gamma \rightarrow M$ direction, and using AGF at a ZnO/ZnO interface, which accounts for the exact geometry of the Brillouin Zone in ZnO. The most accurate calculation for this maximum TBC determined via the AGF calculations sets the upper bound for the ZnO flux, and our data are over a factor of 2 lower than this limit. We note the substantial disagreement between the AGF maximum limit and that calculated via eq 1, which is most likely due to our assumptions of the Brillouin Zone shape and the dispersion relation used to calculate TBC under the DMM framework, as previously discussed. Thus, when determining the maximum possible TBC across interfaces, it is important to use as detailed a phononic spectra as possible to ensure accuracy. Furthermore, even at these heteroepitaxial ZnO/GaN interfaces the measured TBC is only ∼30% of the maximum TBC. Given our previous discussion regarding the high efficacy of long wavelength modes, these data also suggest that high frequency modes are not effective carriers of energy across interfaces, which supports recent computational findings.[56,73]

In summary, we have reported experimental measurements of the TBC across isolated heteroepitaxially grown ZnO films on GaN substrates from 77−500 K, providing a direct comparison of measured TBCs to DMM and AGF simulations. This comparison allows for a direct assessment of the assumptions implemented in DMM and AGF calculations. Our measurements, when compared to previous experimental data across ZnO/HQ/ZnO interfaces, suggest that the TBC can be influenced by the modes in the material on one side as opposed to the "vibrational mismatch" concept assumed in the DMM. Furthermore, the disagreement between both the DMM and AGF, and the experimental data at elevated temperatures, suggests that the contributions associated with anharmonicity and also possibly from other types of modes that are not accounted for in these commonly used harmonic formalisms, are far from negligible. Our data suggest that long wavelength phonons can effectively transmit across interfaces, supporting the findings of recent computational studies.[56,73]

These results also provide invaluable impact into strategies for thermal mitigation and power dissipation in electronic devices such as microprocessors, semiconductor-based radio frequency devices, and radar amplifiers.[81−83] The thermal bottleneck in these devices has proven to be the major roadblock in achieving higher power gallium nitride high-electron mobility transistors (GaN HEMTs) along with other semiconductor-based high-frequency, high-output power technologies.[84,85] A significant limitation in the ability to scale devices to higher powers, especially as active regions continue to dimensionally shrink, is the TBC at GaN interfaces, and its effect on heat transfer into submounts and heat sinks.[86] Our results lend insight into how phonon modes couple energy across GaN-based interfaces.

■ ASSOCIATED CONTENT

Supporting Information

The Supporting Information is available free of charge on the ACS Publications website at DOI: 10.1021/acs.nanolett.8b02837.

Fabrication process; sample characterization with XRD, AFM, and TEM; details of thermal conductivity measurements with TDTR; computational domain setup and methodology for molecular dynamics simulations and lattice dynamics calculations (ZIP)

■ AUTHOR INFORMATION

Corresponding Author

*E-mail: phopkins@virginia.edu.

ORCID

John T. Gaskins: 0000-0001-8622-5902
Ashutosh Giri: 0000-0002-8899-4964
Shenghong Ju: 0000-0001-7863-6947
Zhe Cheng: 0000-0001-7827-2979
Samuel Graham: 0000-0002-1299-1636
Tengfei Luo: 0000-0003-3940-8786

DOI: 10.1021/acs.nanolett.8b02837
Nano Lett. 2018, 18, 7469−7477

Junichiro Shiomi: 0000-0002-3552-4555
Patrick E. Hopkins: 0000-0002-3403-743X

Present Addresses

G.N.K. and J.-P.M.: Department of Materials Science and Engineering, The Pennsylvania State University, University Park, Pennsylvania 16802, United States.
A.R. and A.H.: Department of Mechanical Engineering, Massachusetts Institute of Technology, Cambridge MA, 02139 United States.
B.M.F.: Department of Mechanical and Nuclear Engineering The Pennsylvania State University University Park, Pennsylvania 16802.

Notes

The authors declare no competing financial interest.

■ ACKNOWLEDGMENTS

We appreciate support from the Office of Naval Research under a MURI program, Grant N00014-18-1-2429, the National Science Foundation, Grant 1554050,the Army Research Office, Grant W911NF-16-1-0406, NSF Ceramics, award 1610844, and supported in part by the "Materials Research by Information Integration" Initiative (MI2I) project of the Support Program for Starting Up Innovation Hub from Japan Science and Technology Agency (JST).

■ REFERENCES

(1) Duda, J. C.; Beechem, T. E.; Smoyer, J. L.; Norris, P. M.; Hopkins, P. E. Role of Dispersion on Phononic Thermal Boundary Conductance. *J. Appl. Phys.* **2010**, *108*, 073515.
(2) Wilson, R.; Apgar, B. A.; Hsieh, W.-P.; Martin, L. W.; Cahill, D. G. Thermal Conductance of Strongly Bonded Metal-oxide Interfaces. *Phys. Rev. B: Condens. Matter Mater. Phys.* **2015**, *91*, 115414.
(3) Lyeo, H. K.; Cahill, D. G. Thermal Conductance of Interfaces Between Highly Dissimilar Materials. *Phys. Rev. B: Condens. Matter Mater. Phys.* **2006**, *73*, 144301.
(4) Stevens, R. J.; Smith, A. N.; Norris, P. M. Measurement of Thermal Boundary Conductance of a Series of Metal-dielectric Interfaces by the Transient Thermoreflectance Technique. *J. Heat Transfer* **2005**, *127*, 315−322.
(5) Costescu, R. M.; Wall, M. A.; Cahill, D. G. Thermal Conductance of Epitaxial Interfaces. *Phys. Rev. B: Condens. Matter Mater. Phys.* **2003**, *67*, 054302.
(6) Stoner, R.; Maris, H.; Anthony, T.; Banholzer, W. Measurements of the Kapitza Conductance Between Diamond and Several Metals. *Phys. Rev. Lett.* **1992**, *68*, 1563.
(7) Cho, J.; Li, Y.; Hoke, W. E.; Altman, D. H.; Asheghi, M.; Goodson, K. E. Phonon Scattering in Strained Transition Layers for GaN Heteroepitaxy. *Phys. Rev. B: Condens. Matter Mater. Phys.* **2014**, *89*, 115301.
(8) Swartz, E. T.; Pohl, R. O. Thermal Boundary Resistance. *Rev. Mod. Phys.* **1989**, *61*, 605.
(9) Giri, A.; Niemelä, J.-P.; Tynell, T.; Gaskins, J. T.; Donovan, B. F.; Karppinen, M.; Hopkins, P. E. Heat-transport Mechanisms in Molecular Building Blocks of Inorganic/organic Hybrid Superlattices. *Phys. Rev. B: Condens. Matter Mater. Phys.* **2016**, *93*, 115310.
(10) Gordiz, K.; Henry, A. Phonon Transport at Interfaces: Determining the Correct Modes of Vibration. *J. Appl. Phys.* **2016**, *119*, 015101.
(11) Gordiz, K.; Henry, A. Phonon Transport at Interfaces Between Different Phases of Silicon and Germanium. *J. Appl. Phys.* **2017**, *121*, 025102.
(12) Ye, N.; Feser, J. P.; Sadasivam, S.; Fisher, T. S.; Wang, T.; Ni, C.; Janotti, A. Thermal Transport Across Metal Silicide-silicon Interfaces: An Experimental Comparison Between Epitaxial and Nonepitaxial Interfaces. *Phys. Rev. B: Condens. Matter Mater. Phys.* **2017**, *95*, 085430.
(13) Cheaito, R.; Gaskins, J. T.; Caplan, M. E.; Donovan, B. F.; Foley, B. M.; Giri, A.; Duda, J. C.; Szwejkowski, C. J.; Constantin, C.; Brown-Shaklee, H. J.; Ihlefeld, J. F.; Hopkins, P. E. Thermal Boundary Conductance Accumulation and Interfacial Phonon Transmission: Measurements and Theory. *Phys. Rev. B: Condens. Matter Mater. Phys.* **2015**, *91*, 035432.
(14) Dechaumphai, E.; Lu, D.; Kan, J. J.; Moon, J.; Fullerton, E. E.; Liu, Z.; Chen, R. Ultralow Thermal Conductivity of Multilayers with Highly Dissimilar Debye Temperatures. *Nano Lett.* **2014**, *14*, 2448−2455.
(15) Hopkins, P. E. Thermal Transport Across Solid Interfaces with Nanoscale Imperfections: Effects of Roughness, Disorder, Dislocations, and Bonding on Thermal Boundary Conductance. *ISRN Mechanical Engineering* **2013**, *2013*, 1.
(16) Monachon, C.; Weber, L.; Dames, C. Thermal Boundary Conductance: A Materials Science Perspective. *Annu. Rev. Mater. Res.* **2016**, *46*, 433−463.
(17) Stoner, R. J.; Maris, H. J. Kapitza Conductance and Heat Flow Between Solids at Temperatures From 50 to 300 K. *Phys. Rev. B: Condens. Matter Mater. Phys.* **1993**, *48*, 16373−16387.
(18) Majumdar, A.; Reddy, P. Role of Electron-phonon Coupling in Thermal Conductance of Metal-nonmetal Interfaces. *Appl. Phys. Lett.* **2004**, *84*, 4768−4770.
(19) Wang, Y.; Ruan, X.; Roy, A. K. Two-temperature Nonequilibrium Molecular Dynamics Simulation of Thermal Transport Across Metal-nonmetal Interfaces. *Phys. Rev. B: Condens. Matter Mater. Phys.* **2012**, *85*, 205311.
(20) Lu, Z.; Wang, Y.; Ruan, X. Metal/dielectric Thermal Interfacial Transport Considering Cross-interface Electron-phonon Coupling: Theory, Two-temperature Molecular Dynamics, and Thermal Circuit. *Phys. Rev. B: Condens. Matter Mater. Phys.* **2016**, *93*, 064302.
(21) Ordonez-Miranda, J.; Alvarado-Gil, J. J.; Yang, R. The Effect of the Electron-phonon Coupling on the Effective Thermal Conductivity of Metal-nonmetal Multilayers. *J. Appl. Phys.* **2011**, *109*, 094310.
(22) Sadasivam, S.; Waghmare, U. V.; Fisher, T. S. Electron-phonon Coupling and Thermal Conductance at a Metal-semiconductor Interface: First-principles Analysis. *J. Appl. Phys.* **2015**, *117*, 134502.
(23) Huberman, M. L.; Overhauser, A. W. Electronic Kapitza Conductance at a Diamond-Pb Interface. *Phys. Rev. B: Condens. Matter Mater. Phys.* **1994**, *50*, 2865−2873.
(24) Sergeev, A. V. Electronic Kapitza Conductance Due to Inelastic Electron-boundary Scattering. *Phys. Rev. B: Condens. Matter Mater. Phys.* **1998**, *58*, R10199.
(25) Sergeev, A. V. Inelastic Electron-boundary Scattering in Thin Films. *Phys. B* **1999**, *263−264*, 217−219.
(26) Sergeev, A.; Mitin, V. Electron-phonon Interaction in Disordered Conductors: Static and Vibrating Scattering Potentials. *Phys. Rev. B: Condens. Matter Mater. Phys.* **2000**, *61*, 6041−6047.
(27) Sergeev, A.; Karasik, B. S.; Gershenson, M.; Mitin, V. Electron-phonon Scattering in Disordered Metallic Films. *Phys. B* **2002**, *316-317*, 328−330.
(28) Hohensee, G. T.; Wilson, R. B.; Cahill, D. G. Thermal Conductance of Metal−diamond Interfaces at High Pressure. *Nat. Commun.* **2015**, *6*, 6578.
(29) Giri, A.; Gaskins, J. T.; Donovan, B. F.; Szwejkowski, C.; Warzoha, R. J.; Rodriguez, M. A.; Ihlefeld, J.; Hopkins, P. E. Mechanisms of Nonequilibrium Electron-phonon Coupling and Thermal Conductance at Interfaces. *J. Appl. Phys.* **2015**, *117*, 105105.
(30) Li, X.; Park, W.; Chen, Y. P.; Ruan, X. Absence of Coupled Thermal Interfaces in Al_2O_3/Ni/Al_2O_3 Sandwich Structure. *Appl. Phys. Lett.* **2017**, *111*, 143102.
(31) Hopkins, P. E.; Serrano, J. R.; Phinney, L. M.; Kearney, S. P.; Grasser, T. W.; Harris, C. T. Criteria for Cross-plane Dominated Thermal Transport in Multilayer Thin Film Systems During Modulated Laser Heating. *J. Heat Transfer* **2010**, *132*, 081302.
(32) Hopkins, P. E.; Duda, J. C.; Clark, S. P.; Hains, C. P.; Rotter, T. J.; Phinney, L. M.; Balakrishnan, G. Effect of Dislocation Density on Thermal Boundary Conductance Across GaSb/GaAs Interfaces. *Appl. Phys. Lett.* **2011**, *98*, 161913.

DOI: 10.1021/acs.nanolett.8b02837
Nano Lett. 2018, 18, 7469−7477

(33) Kimling, J.; Philippi-Kobs, A.; Jacobsohn, J.; Oepen, H. P.; Cahill, D. G. Thermal Conductance of Interfaces with Amorphous SiO_2 Measured by Time-resolved Magneto-optic Kerr-effect Thermometry. *Phys. Rev. B: Condens. Matter Mater. Phys.* **2017**, *95*, 184305.
(34) Zhu, J.; Tang, D.; Wang, W.; Liu, J.; Holub, K. W.; Yang, R. Ultrafast Thermoreflectance Techniques for Measuring Thermal Conductivity and Interface Thermal Conductance of Thin Films. *J. Appl. Phys.* **2010**, *108*, 094315.
(35) Collazo, R.; Mita, S.; Aleksov, A.; Schlesser, R.; Sitar, Z. Growth of Ga-and N-polar Gallium Nitride Layers by Metalorganic Vapor Phase Epitaxy on Sapphire Wafers. *J. Cryst. Growth* **2006**, *287*, 586−590.
(36) Mita, S.; Collazo, R.; Rice, A.; Dalmau, R.; Sitar, Z. Influence of Gallium Supersaturation on the Properties of GaN Grown by Metalorganic Chemical Vapor Deposition. *J. Appl. Phys.* **2008**, *104*, 013521.
(37) Kato, N.; Lang, A. A Study of Pendellösung Fringes in X-ray Diffraction. *Acta Crystallogr.* **1959**, *12*, 787−794.
(38) Wainfan, N.; Parratt, L. X-Ray Reflection Studies of the Anneal and Oxidation of Some Thin Solid Films. *J. Appl. Phys.* **1960**, *31*, 1331−1337.
(39) Cahill, D. G. Analysis of Feat Flow in Layered Structures for Time-domain Thermoreflectance. *Rev. Sci. Instrum.* **2004**, *75*, 5119−5122.
(40) Schmidt, A. J.; Chen, X.; Chen, G. Pulse Accumulation, Radial Heat Conduction, and Anisotropic Thermal Conductivity in Pump-probe Transient Thermoreflectance. *Rev. Sci. Instrum.* **2008**, *79*, 114902.
(41) Beechem, T. E.; McDonald, A. E.; Fuller, E. J.; Talin, A. A.; Rost, C. M.; Maria, J.-P.; Gaskins, J. T.; Hopkins, P. E.; Allerman, A. A. Size Dictated Thermal Conductivity of GaN. *J. Appl. Phys.* **2016**, *120*, 095104.
(42) Alvarez-Quintana, J.; Martínez, E.; Pérez-Tijerina, E.; Pérez-García, S.; Rodríguez-Viejo, J. Temperature Dependent Thermal Conductivity of Polycrystalline ZnO Films. *J. Appl. Phys.* **2010**, *107*, 063713.
(43) Tsubota, T.; Ohtaki, M.; Eguchi, K.; Arai, H. Thermoelectric Properties of Al-doped ZnO as a Promising Oxide Material for High-temperature Thermoelectric Conversion. *J. Mater. Chem.* **1997**, *7*, 85−90.
(44) Barrado, C.; Leite, E.; Bueno, P. R.; Longo, E.; Varela, J. A. Thermal Conductivity Features of ZnO-based Varistors Using the Laser-pulse Method. *Mater. Sci. Eng., A* **2004**, *371*, 377−381.
(45) Wu, X.; Lee, J.; Varshney, V.; Wohlwend, J. L.; Roy, A. K.; Luo, T. Thermal Conductivity of Wurtzite Zinc-oxide from First-principles Lattice Dynamics - a Comparative Study with Gallium Nitride. *Sci. Rep.* **2016**, *6*, 22504.
(46) Huang, Z. X.; Tang, Z. A.; Yu, J.; Bai, S. Thermal Conductivity of Nanoscale Polycrystalline ZnO Thin Films. *Phys. B* **2011**, *406*, 818−823.
(47) Xu, Y.; Goto, M.; Kato, R.; Tanaka, Y.; Kagawa, Y. Thermal Conductivity of ZnO Thin Film Produced by Reactive Sputtering. *J. Appl. Phys.* **2012**, *111*, 084320.
(48) Zeng, T.; Chen, G. Phonon Heat Conduction in Thin Films: Impacts of Thermal Boundary Resistance and Internal Heat Generation. *J. Heat Transfer* **2001**, *123*, 340−347.
(49) Dobrovinskaya, E. R.; Lytvynov, L. A.; Pishchik, V. *Sapphire: Material, Manufacturing, Applications*; Springer Science & Business Media, 2009.
(50) Ditmars, D.; Ishihara, S.; Chang, S.; Bernstein, G.; West, E. Enthalpy and Heat-capacity Standard Reference Material: Synthetic Sapphire (a-Al2O3) from 10 to 2250 K. *J. Res. Natl. Bur. Stand.* **1982**, *87*, 159−163.
(51) Kremer, R.; Cardona, M.; Schmitt, E.; Blumm, J.; Estreicher, S.; Sanati, M.; Bockowski, M.; Grzegory, I.; Suski, T.; Jezowski, A. Heat Capacity of α-GaN: Isotope Effects. *Phys. Rev. B: Condens. Matter Mater. Phys.* **2005**, *72*, 075209.
(52) Simon, R. B.; Anaya, J.; Kuball, M. Thermal Conductivity of Bulk GaN—Effects of Oxygen, Magnesium Doping, and Strain Field Compensation. *Appl. Phys. Lett.* **2014**, *105*, 202105.
(53) *II-VI and I-VII Compounds; Semimagnetic Compounds*; Madelung, O., Rössler, U., Schulz, M., Eds.; Springer Berlin Heidelberg: Berlin, Heidelberg, 1999; pp 1−5.
(54) Corruccini, R. J.; Gniewek, J. J. *SPECIFIC HEATS AND ENTHALPIES OF TECHNICAL SOLIDS AT LOW TEMPERATURES. A Compilation from the Literature*; National Bureau of Standards, Washington, DC., 1960.
(55) Duda, J. C.; Norris, P. M.; Hopkins, P. E. On the Linear Temperature Dependence of Phonon Thermal Boundary Conductance in the Classical Limit. *J. Heat Transfer* **2011**, *133*, 074501.
(56) Hua, C.; Chen, X.; Ravichandran, N. K.; Minnich, A. J. Experimental Metrology to Obtain Thermal Phonon Transmission Coefficients at Solid Interfaces. *Phys. Rev. B: Condens. Matter Mater. Phys.* **2017**, *95*, 205423.
(57) Imry, Y.; Landauer, R. Conductance Viewed as Transmission. *Rev. Mod. Phys.* **1999**, *71*, S306−S312.
(58) Duda, J. C.; Hopkins, P. E.; Smoyer, J. L.; Bauer, M. L.; English, T. S.; Saltonstall, C. B.; Norris, P. M. On the Assumption of Detailed Balance in Prediction of Diffusive Transmission Probability During Interfacial Transport. *Nanoscale Microscale Thermophys. Eng.* **2010**, *14*, 21−33.
(59) Ruf, T.; Serrano, J.; Cardona, M.; Pavone, P.; Pabst, M.; Krisch, M.; D'astuto, M.; Suski, T.; Grzegory, I.; Leszczynski, M. Phonon Dispersion Curves in Wurtzite-Structure GaN Determined by Inelastic X-ray Scattering. *Phys. Rev. Lett.* **2001**, *86*, 906.
(60) Serrano, J.; Manjón, F.; Romero, A.; Ivanov, A.; Cardona, M.; Lauck, R.; Bosak, A.; Krisch, M. Phonon Dispersion Relations of Zinc Oxide: Inelastic Neutron Scattering and Ab Initio Calculations. *Phys. Rev. B: Condens. Matter Mater. Phys.* **2010**, *81*, 174304.
(61) Duda, J. C.; Smoyer, J. L.; Norris, P. M.; Hopkins, P. E. Extension of the Diffuse Mismatch Model for Thermal Boundary Conductance Between Isotropic and Anisotropic Materials. *Appl. Phys. Lett.* **2009**, *95*, 031912.
(62) Duda, J. C.; Hopkins, P. E.; Beechem, T. E.; Smoyer, J. L.; Norris, P. M. Inelastic Phonon Interactions at Solid-graphite Interfaces. *Superlattices Microstruct.* **2010**, *47*, 550−555.
(63) Hopkins, P. E.; Beechem, T. E.; Duda, J. C.; Hattar, K.; Ihlefeld, J. F.; Rodriguez, M. A.; Piekos, E. S. Influence of Anisotropy on Thermal Boundary Conductance at Solid Interfaces. *Phys. Rev. B: Condens. Matter Mater. Phys.* **2011**, *84*, 125408.
(64) Chen, Z.; Wei, Z.; Chen, Y.; Dames, C. Anisotropic Debye Model for the Thermal Boundary Conductance. *Phys. Rev. B: Condens. Matter Mater. Phys.* **2013**, *87*, 125426.
(65) Giannozzi, P.; Baroni, S.; Bonini, N.; Calandra, M.; Car, R.; Cavazzoni, C.; Ceresoli, D.; Chiarotti, G. L.; Cococcioni, M.; Dabo, I.; et al. QUANTUM ESPRESSO: a Modular and Open-source Software Project for Quantum Simulations of Materials. *J. Phys.: Condens. Matter* **2009**, *21*, 395502.
(66) Wang, J.-S.; Wang, J.; Zeng, N. Nonequilibrium Green's Function Approach to Mesoscopic Thermal Transport. *Phys. Rev. B: Condens. Matter Mater. Phys.* **2006**, *74*, 033408.
(67) Zhang, W.; Fisher, T.; Mingo, N. The Atomistic Green's Function Method: An Efficient Simulation Approach for Nanoscale Phonon Transport. *Numer. Heat Transfer, Part B* **2007**, *51*, 333−349.
(68) Tian, Z.; Esfarjani, K.; Chen, G. Enhancing Phonon Transmission Across a Si/Ge Interface by Atomic Roughness: First-principles Study with the Green's Function Method. *Phys. Rev. B: Condens. Matter Mater. Phys.* **2012**, *86*, 235304.
(69) Li, X.; Yang, R. Size-dependent Phonon Transmission Across Dissimilar Material Interfaces. *J. Phys.: Condens. Matter* **2012**, *24*, 155302.
(70) Little, W. A. The Transport of Heat Between Dissimilar Solids at Low Temperatures. *Can. J. Phys.* **1959**, *37*, 334−349.
(71) Snyder, N. S. Heat Transport Through Helium II: Kapitza Conductance. *Cryogenics* **1970**, *10*, 89−95.

DOI: 10.1021/acs.nanolett.8b02837
Nano Lett. 2018, 18, 7469−7477

(72) Hopkins, P. E.; Norris, P. M.; Tsegaye, M. S.; Ghosh, A. W. Extracting Phonon Thermal Conductance Across Nanoscale Junctions: Nonequilibrium Green's Function Approach Compared to Semi-classical Methods. *J. Appl. Phys.* **2009**, *106*, 063503.
(73) Latour, B.; Shulumba, N.; Minnich, A. J. Ab Initio Study of Mode-resolved Phonon Transmission at Si/Ge Interfaces Using Atomistic Green's Functions. *Phys. Rev. B: Condens. Matter Mater. Phys.* **2017**, *96*, 104310.
(74) Hopkins, P. E.; Duda, J. C.; Petz, C. W.; Floro, J. A. Controlling Thermal Conductance Through Quantum Dot Roughening at Interfaces. *Phys. Rev. B: Condens. Matter Mater. Phys.* **2011**, *84*, 035438.
(75) Duda, J. C.; Hopkins, P. E. Systematically Controlling Kapitza Conductance via Chemical Etching. *Appl. Phys. Lett.* **2012**, *100*, 111602.
(76) Hopkins, P. E. Multiple Phonon Processes Contributing to Inelastic Scattering During Thermal Boundary Conductance at Solid Interfaces. *J. Appl. Phys.* **2009**, *106*, 013528.
(77) Hopkins, P. E.; Duda, J. C.; Norris, P. M. Anharmonic Phonon Interactions at Interfaces and Contributions to Thermal Boundary Conductance. *J. Heat Transfer* **2011**, *133*, 062401.
(78) Hopkins, P. E.; Stevens, R. J.; Norris, P. M. Influence of Inelastic Scattering at Metal-dielectric Interfaces. *J. Heat Transfer* **2008**, *130*, 022401.
(79) Panzer, M. A.; Duong, H. M.; Shiomi, J.; Wardle, B. L.; Maruyama, S.; Goodson, K. E.; et al. Temperature-dependent Phonon Conduction and Nanotube Engagement in Metalized Single Wall Carbon Nanotube Films. *Nano Lett.* **2010**, *10*, 2395−2400.
(80) Sääskilahti, K.; Oksanen, J.; Tulkki, J.; Volz, S. Role of Anharmonic Phonon Scattering in the Spectrally Decomposed Thermal Conductance at Planar Interfaces. *Phys. Rev. B: Condens. Matter Mater. Phys.* **2014**, *90*, 134312.
(81) Smith, A.; Calame, J. Impact of Thin Film Thermophysical Properties on Thermal Management of Wide Bandgap Solid-state Transistors. *Int. J. Thermophys.* **2004**, *25*, 409−422.
(82) Trew, R. SiC and GaN Transistors - Is There One Winner for Microwave Power Applications? *Proc. IEEE* **2002**, *90*, 1032−1047.
(83) Lin, S.-C.; Banerjee, K. Cool chips: Opportunities and Implications for Power and Thermal Management. *IEEE Trans. Electron Devices* **2008**, *55*, 245−255.
(84) Mishra, U. K.; Parikh, P.; Wu, Y.-F. AlGaN/GaN HEMTs - an Overview of Device Operation and Applications. *Proc. IEEE* **2002**, *90*, 1022−1031.
(85) Zhou, Q.; Cross, A. S.; Fu, Y.; Beling, A.; Foley, B. M.; Hopkins, P. E.; Campbell, J. C. Balanced InP/InGaAs Photodiodes with 1.5-W Output Power. *IEEE Photonics J.* **2013**, *5*, 6800307−6800307.
(86) Cho, J.; Li, Z.; Bozorg-Grayeli, E.; Kodama, T.; Francis, D.; Ejeckam, F.; Faili, F.; Asheghi, M.; Goodson, K. E. Improved Thermal Interfaces of GaN−diamond Composite Substrates for HEMT Applications. *IEEE Trans. Compon., Packag., Manuf. Technol.* **2013**, *3*, 79−85.

DOI: 10.1021/acs.nanolett.8b02837
Nano Lett. 2018, 18, 7469−7477